

# A novel scatter correction method for Cone Beam Computed Tomography

Kun Zhou<sup>\*</sup>, Zhaoheng Xie<sup>\*</sup>, Yanye Lu<sup>\*§</sup>, Kun Yang<sup>¶</sup>, Qiushi Ren<sup>\*</sup>

<sup>\*</sup>Department of Biomedical Engineering, Peking University, Beijing, China

<sup>¶</sup>College of Quality and Technical Supervision, Hebei University, Baoding, China

<sup>§</sup>Pattern Recognition Lab, Department of Computer Science,

Friedrich-Alexander-University Erlangen-Nuremberg, Erlangen, Germany

**Abstract—Abstract---** In this paper, we proposed a novel scatter correction approach for cone beam computed tomography based on Klein-Nishina formulation. Also a principle was proposed that the photons intensity distribution was determined by the attenuation coefficient  $\mu$  and the path length  $l$  by deducting this formulation, which declares that two pencil beams pass through two objects with the same values of  $\mu l$  could result in same photons intensity distribution, i.e., point spread function (PSF), even if the corresponding  $\mu$  and  $l$  are different. The simulation and experimental results demonstrated the feasibility of our approach, as well as the comparison with the beam stop array (BSA) method for evaluation.

**Index Terms—**Scatter, Klein-Nishina, CBCT

## I. INTRODUCTION

OWING to the rapid scanning process and sufficient X-ray utilization, cone beam computed tomography (CBCT), a technology on the frontier of medical imaging research, has also been applied in various areas such clinical diagnostics and basic research. However, during the imaging process of the CBCT, Compton scattering contributed by the interaction between the X-ray and the material causes scattering artifacts, which decreases the image contrast and resolution, resulting in negative effect to diagnosis[1]. Since higher imaging quality is required in applied CBCT systems, scatter artifacts have to be corrected before or during image reconstruction. Many scatter correction methods have been proposed in literatures[2], and J. Boone has classified them into two categories: software correction and hardware correction[3].

## II. METHODS

### A. Approach derivation

According to Klein-Nishina scatter cross section formula, the

relationship between the photons intensity distribution, which is represented by point spread function (PSF), and the geometry parameters, the physical properties of the object could be derived. Here the full width tenth maximum (FWTM) was adopted to indicate the cut-off frequency of the PSF. It is noted that here we just take the single scatter into consideration and spectral effects is not considered. When considering small percentage of Rayleigh scattering, the possibility that the incident photon reaching the point  $P(r, \varphi)$  can be calculated by Eq. 1.

$$g'(r, \varphi) = K \int_{s=0}^l \exp[-\mu_s(t-s)]f(\theta)ds \quad (1)$$

$$f(\theta) = \exp\left(\frac{-\mu_s s}{\cos \theta}\right) \times (\sin \theta P(E_\gamma, \theta)^2 [P(E_\gamma, \theta) + \frac{1}{P(E_\gamma, \theta)} - \sin^2 \theta] / 2 \times \left(\frac{\tan \theta}{r(1 + (\tan \theta)^2)}\right)) / 2\pi r \quad (2)$$

where  $K$  is the global constant encompassing several constant terms and  $g'(r, \varphi)$  means the probability of the incident photon reaching the point  $P(r, \varphi)$ . It is easy to find that  $f(\theta)$  is monotone decreasing with the parameter  $\theta$ . As a result,  $g'(r, \varphi)$  is monotone decreasing with the parameter  $r$ . This complies with the laws of PSF. Besides, it is obvious to take  $\mu_s s$  as one variable. Though the integral variable  $s$  occurs alone somewhere without the attenuation coefficient  $\mu_s$ , however, when it occurs with the air gap  $g$ , which is much larger than  $s$ , as a result, it is reasonable to omit  $s$  occurring alone. So, the Eq. 2 is simplified to be:

$$f(\theta) = \exp\left(\frac{-\mu_s s}{\cos \theta}\right) \times (\sin \theta P(E_\gamma, \theta))^2 \times [P(E_\gamma, \theta) + \frac{1}{P(E_\gamma, \theta)} - \sin^2 \theta] / 2 \times \left(\frac{\tan \theta}{r(1 + (\tan \theta)^2)}\right) / 2\pi r \quad (3)$$

Till now an inference can be summarized that  $g'(r, \varphi)$  has one-to-one mapping relationship with  $\mu_s t$ , and the larger  $\mu_s t$  the larger FWTM of the  $PSF$ .

As is known to everybody, the intensity detected by the X-ray detector contains both the real information and the scatter information, which can be delineated by:

$$I_1 = I_{real} + I_{scatter} \quad (4)$$

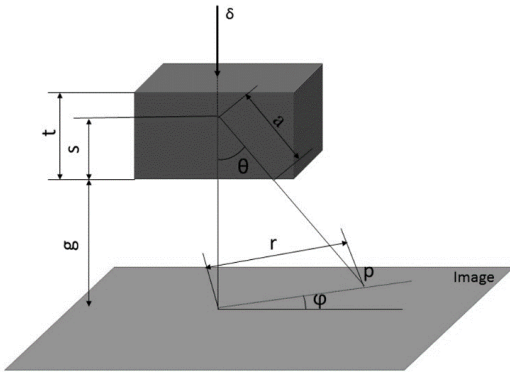


Figure 1. The X-ray scatter schematic diagram used to derive the  $PSF$ : a photon enters the object perpendicularly from the position  $\delta$ , and scatters at the position  $a$  distance of  $s$  from the bottom surface. The scatter angle is  $\theta$ , the air gap is  $g$ . The photon reaches the image plane at the position  $P(r, \varphi)$

where  $I_1, I_{real}, I_{scatter}$  are matrices with a dimension of  $m \times n$  and indicate the detected information, real information and scatter information respectively. If  $I_{real}$  and the  $PSF$  of each point of  $I_{real}$  are known,  $I_{scatter}$  can be calculated by the following equation:

$$I_{scatter}(i, j) = \sum_{p=1}^m \sum_{t=1}^n I_{real}(p, t) \times PSF\left(i + \frac{m_{psf}}{2} - p + 1, j + \frac{n_{psf}}{2} - t + 1\right) \quad (5)$$

$$PSF(i < 0, j < 0) = 0$$

where  $I_{scatter}(i, j)$  means the value of  $I_{scatter}$  at position

$(i, j)$  while  $PSF(i, j)$  indicates the  $PSF$  at the position  $(i, j)$ , namely, when the incident photons enter the object along the direction of the source point to the position  $(i, j)$ , it will have the corresponding  $PSF$ . Here  $PSF$  is defined as a matrix with a dimension of  $m_{psf} \times n_{psf}$ . However, in practice, all these are unknown, so we should substitute these parameters with some parameters that are already known or could be measured. So here, we substitute the  $I_{real}$  with  $I_1$  as the scatter fraction does not change the characteristic of real information so much due to the low frequency of the scatter information. As to the  $PSF$  processing, the threshold segmentation is conducted on  $I_1$ . According to our inference, the same  $\mu_s t$ , results in the same  $PSF$ . As a result, only one  $PSF$  is needed by each segment, which greatly reduces the complexity of the calculation and it also enabled highly paralleled calculation, because each segment could be organized parallel to the each other, and in the same segment, each point could be organized parallel to each other as  $PSF$  is the same within a segment. There are many types of  $PSF$  to choose from, such as Gaussian function and Poisson function, etc. The cutoff frequency of the  $PSF$ , namely the FWTM of the  $PSF$  needs to be determined. Because of the one-to-one map relationship between the  $PSF$  and  $\mu_s t$ , lots of  $PSF$  could be obtained through Monte Carlo simulation with different  $\mu_s t$ . It is very easy to construct a database, which shows the value of  $\mu_s t$  and the corresponding  $PSF$ .

## B. Phantom study

A standard QRM scatter phantom and a BSA (Beam Stop Array) phantom were used to testify the effect of the scatter correction method. The phantom structure and geometric parameters are shown in Fig. 2.

360 projection images with and without a BSA phantom were obtained with one full angle scan. The BSA phantom was placed between the X-ray source and the object. The distance from the X-ray spot to the rotation axis and the detector was 375mm and 625mm respectively and the BSA phantom was approximately 50mm to the rotation axis. Once the projection images with BSA phantom were obtained, the scatter fraction was obtained by the typical method proposed by R. Ning. The projection images obtained without BSA phantom were segmented to two parts because of the simple structure of the phantom. The principle of the segmentation is that both of the

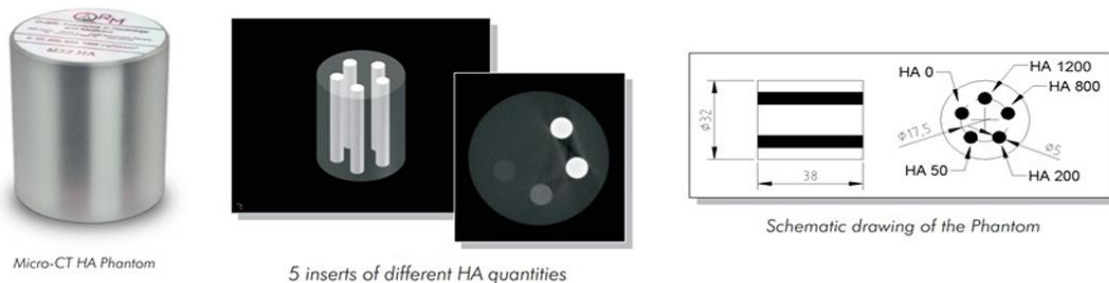


Figure 2. The QRM scatter phantom

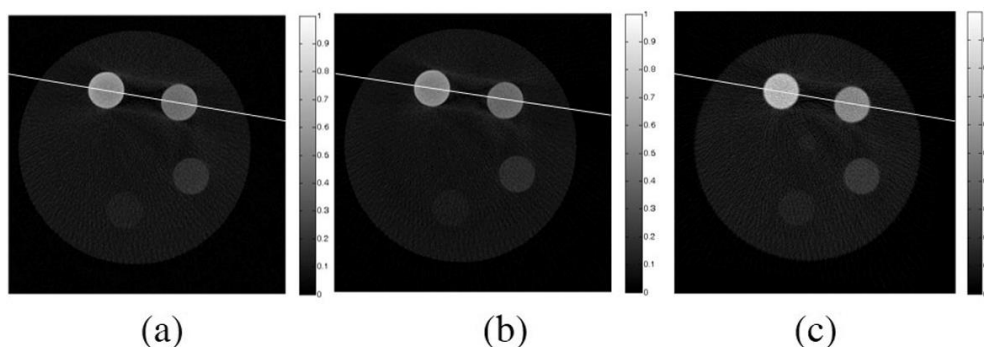


Figure 3. The image reconstruction of the QRM scatter phantom (a) without scatter correction, (b) with scatter correction with our method, and (c) with scatter correction with BSA method.

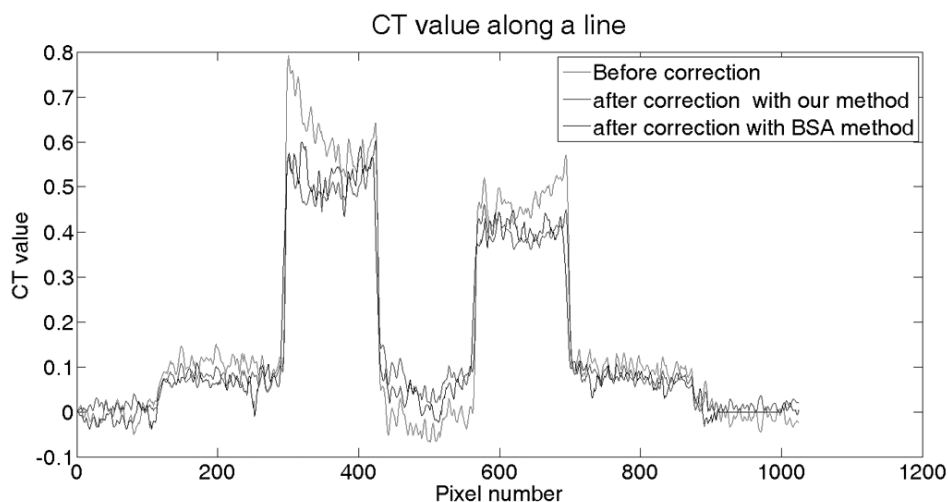


Figure 4. The corresponding pixel values along the lines drawn in Fig 3.

two parts are approximately half of the initial image. Then the scatter matrix was obtained by Eq. 13 with the FWTM of the PSF set to be (89,169) according to the Monte Carlo simulation database, which means the FWTM of the PSF is 89 pixel size to lower  $\mu_s t$  and 169 pixel size to higher  $\mu_s t$  as our detector is 1944\*1536 size with a 0.0748mm pixel size. Here, Our PSF assumed a Gaussian form as the simulation experiment shows a good Gaussian linefit. After the scatter fraction elimination, the corrected projection images (our method and BSA method) were reconstructed to a 1024\*1024\*1024 size image using FDK reconstruction method with geometry calibration respectively.

### III. RESULTS

The reconstruction results are shown in Fig 3 and Fig 4. Fig3 shows the reconstructed images with and without scatter correction while Fig 4 shows corresponding pixel value along a line drawn in Fig 3 (the line pass through the two brightest discs). The line in all of the images share the same position.

### IV. CONCLUSION

It is obviously to see that the image quality improvement after the scatter correction and image quality with scatter correction using our approach is comparable to image quality with the BSA method from Fig 3, 4. Fig 3 intuitive shows the image quality improvement, especially in the region around the

brightest discs, where the scatter artifacts is much more serious when compare Fig 3(a) with Fig 3(b), (c). Fig 4 shows the homogeneity of the image through the CT value along the line that pass through the center of the two brightest discs. It is easy to find that the homogeneity is much better after scatter correction, and the homogeneity of the image obtained with scatter correction through our approach and BSA method are comparable.

### REFERENCES

- [1] A. L. Kwan, J. M. Boone, and N. Shah, "Evaluation of x-ray scatter properties in a dedicated cone-beam breast CT scanner," *Medical physics*, vol. 32, pp. 2967-2975, 2005.
- [2] J. Siewerdsen, M. Daly, B. Bakhtiar, D. Moseley, S. Richard, H. Keller, *et al.*, "A simple, direct method for x-ray scatter estimation and correction in digital radiography and cone-beam CT," *Medical physics*, vol. 33, pp. 187-197, 2006.
- [3] J. M. Boone, "Scatter correction algorithm for digitally acquired radiographs: Theory and results," *Medical physics*, vol. 13, pp. 319-328, 1986.